INTERNATIONAL JOURNAL OF
NUMERICAL ANALYSIS AND MODELING
Volume 10, Number 2, Pages 389–410

AN OPTIMAL 9-POINT FINITE DIFFERENCE SCHEME FOR THE HELMHOLTZ EQUATION WITH PML

ZHONGYING CHEN[†], DONGSHENG CHENG[†],WEI FENG[†] AND TINGTING WU [‡,†]

Abstract. In this paper, we analyze the defect of the rotated 9-point finite difference scheme, and present an optimal 9-point finite difference scheme for the Helmholtz equation with perfectly matched layer (PML) in two dimensional domain. For this method, we give an error analysis for the numerical wavenumber's approximation of the exact wavenumber. Moreover, based on minimizing the numerical dispersion, we propose global and refined choice strategies for choosing optimal parameters of the 9-point finite difference scheme. Numerical experiments are given to illustrate the improvement of the accuracy and the reduction of the numerical dispersion.

Key words. Helmholtz equation, PML, 9-point finite difference scheme, numerical dispersion.

1. Introduction

The Helmholtz equation

$$-\Delta u - k^2 u = f, \tag{1.1}$$

governs wave propagations and scattering phenomena arising in many areas, for example, in aeronautics, marine technology, geophysics and optical problems. In practice, wave equation modeling in the frequency domain has many advantages over time domain modeling. For example, for certain geometries, only a few frequency components are required to perform wave equation inversion and tomography. Moreover, each frequency can be computed independently, which favors parallel computing. Multiexperiment seismic data can also be simulated economically once the impedance matrix is factored. In addition, modeling the effects of attenuation is more flexible in the frequency domain than in the time domain, because in the frequency domain we can directly input the attenuation coefficient as a function of frequency.

To compute the solution of the above problem, due to finite memory of the computer, absorbing boundary conditions are needed to truncate the infinite domain into a finite domain, such as one-way approximation (cf. [6, 7, 10]), PML (cf. [4, 5, 15, 26, 30, 31, 33]), and so on. In this paper, PML is used to truncate the domain and absorb the outgoing waves. The technique of PML was proposed by Bérenger in 1994 (see, [4]). PML has the astonishing property of generating almost no reflection in theory at the interface between the interior medium (the interested domain) and the artificial absorbing medium. The key idea of the PML technique is to introduce an artificial layer with an attenuation parameter around the interior area. The magnitude of the wave is attenuated in the layer while the phase of the wave is conserved. After adding PML to the interior domain, we can impose boundary conditions, like Dirichlet boundary condition, Robin boundary condition and so on, on the outer boundary. Then we obtain a bounded boundary problem, which is usually inverted but ill-conditioned. We refer the interested readers to the

Received by the editors October 13, 2011 and, in revised form, March 3, 2012.
2000 *Mathematics Subject Classification.* 65N06, 65N22, 35L05.

paper [30] for the solvability and the uniqueness for the Helmholtz equation with PML.

For many years, finite difference methods (cf. [3, 11, 14, 16, 19, 24, 25, 26, 27, 32]) and finite element methods (cf. [1, 2, 8, 12, 17]) have been widely used to discrete the Helmholtz equation (1.1). As is known to all, the solution of the Helmholtz equation oscillates severely for large wavenumbers, and the quality of the numerical results usually deteriorates as the wavenumber k increasing (cf. [1, 2, 8, 12, 17]). Hence, there is a growing interest in discretization methods where the computational complexity increases only moderately with increasing wavenumber (cf. [1, 12, 13, 19, 25]).

Finite-difference frequency-domain modeling for the generation of synthetic seismograms and crosshole tomography has been an active field of research since the 1980s (see, [25]). Finite difference methods are easily implemented and its computational complexity is much less than that of finite element methods, although the finite difference method's accuracy is usually lower than that of the finite element method. In addition, by optimizing the parameters in the finite difference formulas, we can easily minimize the numerical dispersion (see, [19, 25]). For accurate modeling, the conventional 5-point finite difference scheme requires 10 gridpoints per wavelength. Therefore, for the Helmholtz equation with large wavenumbers, the resulting matrix is very large and ill-conditioned. Usually, direct methods do not perform well, and iterative methods with preconditioners are alterative (cf. [9, 11, 32]). In 1996, Jo, Shin and Suh proposed the rotated 9-point finite difference scheme for the Helmholtz equation (see, [19]). The approach consists of linearly combining the two discretizations of the second derivative operator on the classical Cartesian coordinate system and the 45^o rotated system. They also gave a group of optimal parameters based on the normalized phase velocity. This optimal 9-point scheme reduces the number of gridpoints per wavelength to 5 while preserving the accuracy of the conventional 5-point scheme with 10 gridpoints per wavelength. Therefore, computer memory and CPU time are saved. In 1998, Shin and Sohn extended the idea of the rotated 9-point scheme to the 25-point formula, and they obtained a group of optimal parameters by the singular-value decomposition method (see, [25]). Furthermore, the 25-point formula reduces the number of gridpoints per wavelength to 2. However, the resulting matrix's bandwidth is much wider than that of the 9-point scheme, and there are some difficulties when considering the absorbing conditions. To reduce the numerical error, higher-order finite difference schemes (cf. [3, 26]) were also constructed and widely used. However, to obtain higher-order accuracy, the higher-order schemes require the source term to be smooth enough. Many the practical problems (cf. [22, 23]) are not the case. On the other hand, though that the rotated difference scheme is a popular solver for the Helmholtz equation, it is not a good choice for the Helmholtz equation with PML. We shall illustrate this in detail in this paper.

This paper is organized as follows. In Section 2, we investigate the rotated 9-point finite difference scheme and show that it is not pointwise consistent with the Helmholtz equation with PML. In Section 3, we present a 9-point difference scheme by using the approach suggested in [26], and prove that it is consistent with the Helmholtz equation with PML and is a second order scheme. For this 9-point difference scheme, we then analyze the error between the numerical wavenumber and the exact wavenumber, and propose global and refined choice strategies for choosing optimal parameters of the scheme based on minimizing the numerical dispersion. In Section 4, numerical experiments are given to demonstrate the efficiency of the

scheme. We show that the scheme proposed in Section 3 improves the accuracy and reduces the numerical dispersion significantly. Finally, Section 5 contains the conclusions of this paper.

2. The Rotated 9-point Finite Difference Scheme for the Helmholtz Equation with PML

In this section, we investigate the rotated 9-point finite difference scheme for the Helmholtz equation with PML.

We start with describing the Helmholtz equation with PML [26, 31]. Consider the Helmholtz equation

$$\Delta u + k^2 u = 0, \quad \text{in } \mathbb{R}^2,$$

where $\Delta := \partial^2/\partial x^2 + \partial^2/\partial y^2$ is the Laplacian, k is the wavenumber defined as $k := 2\pi f/v$ in which f and v represent the frequency and the velocity respectively, and u is the unknown indicating the pressure of the wave field.

Applying PML technique to truncate the infinite domain into a bounded rectangular domain leads to the equation

$$\frac{\partial}{\partial x}\left(\frac{e_y}{e_x}\frac{\partial u}{\partial x}\right) + \frac{\partial}{\partial y}\left(\frac{e_x}{e_y}\frac{\partial u}{\partial y}\right) + e_x e_y k^2 u = 0,$$

where $e_x := 1 - i\frac{\sigma_x}{\omega}, e_y := 1 - i\frac{\sigma_y}{\omega}$, in which $\omega := 2\pi f$ denotes the angular frequency, σ_x and σ_y are usually chosen as a differentiable function only depending on the variable x and y respectively for the end of reducing the numerical reflection. Specially,

$$\sigma_x := \begin{cases} 2\pi a_0 f_0 \left(\frac{l_x}{L_{PML}}\right)^2, & \text{inside PML,} \\ 0, & \text{outside PML,} \end{cases}$$

where f_0 is the dominant frequency of the source, L_{PML} is the thickness of PML, and l_x is the distance from the point (x, y) inside PML and the interface between the interior region and PML region. Moreover, a_0 is a constant, and we choose $a_0 = 1.79$ according to the paper [33]. σ_y can be chosen similarly. Denote

$$A := \frac{e_y}{e_x}, \quad B := \frac{e_x}{e_y}, \quad \text{and } C := e_x e_y,$$

then we have

$$\frac{\partial}{\partial x}\left(A\frac{\partial u}{\partial x}\right) + \frac{\partial}{\partial y}\left(B\frac{\partial u}{\partial y}\right) + Ck^2 u = 0. \tag{2.1}$$

Equation (2.1) can be seen as a general form of the Helmholtz equation (1.1) with its corresponding PML, since in the interior domain, $e_x \equiv 1$ and $e_y \equiv 1$ lead to $A = B = C = 1$. We call it the Helmholtz-PML equation. Here, we note that Equation (2.1) is also valid for variable $k(x, y)$ (see, [20, 21]).

We next study the rotated 9-point finite difference scheme (see, [19]). We consider the network of grid points (x_m, y_n), where $x_m := x_0 + (m-1)h$ and $y_n := y_0 + (n-1)h$. Notice that the same step size $h := \Delta x = \Delta y$ is used for both variables x and y. Let $u_{m,n} := u\mid_{x=x_m,y=y_n}$ represent the pressure of the wave field at the location (x_m, y_n), and similarly let $k_{m,n} := k\mid_{x=x_m,y=y_n}$. The key idea of the rotated 9-point scheme is to approximate Δu by a second order centered difference using both the 5-point 0^o star and the 45^o rotated star (see Figure 1(a) and (b)):

$$\begin{aligned} \Delta u\mid_{x=x_m,y=y_n} \approx \Delta_h u\mid_{x=x_m,y=y_n} := \; & a\Delta_{h,0^o} u\mid_{x=x_m,y=y_n} \\ & +(1-a)\Delta_{h,45^o} u\mid_{x=x_m,y=y_n}, \end{aligned} \tag{2.2}$$

where

$$\Delta_{h,0^o} u \mid_{x=x_m,y=y_n} := \frac{1}{h^2}\left\{u_{m-1,n} + u_{m+1,n} + u_{m,n-1} + u_{m,n+1} - 4u_{m,n}\right\},$$

$$\Delta_{h,45^o} u \mid_{x=x_m,y=y_n} := \frac{1}{2h^2}\{u_{m-1,n+1} + u_{m+1,n-1} + u_{m-1,n-1} + u_{m+1,n+1} - 4u_{m,n}\},$$

and $a \in (0, 1]$ is a parameter.

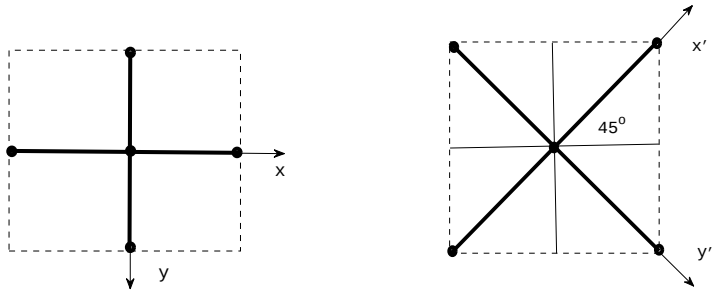

(a) (b)

FIGURE 1. (a) Conventional 0^o five-point star, (b) 45^o rotated star.

In order to approximate the term of zero order with 9 points, we let

$$\begin{aligned}
\mathcal{I}_{h,0^o}\left(k^2u\right) \mid_{x=x_m,y=y_n} &:= \frac{1}{4}\Big(k^2_{m-1,n}u_{m-1,n} + k^2_{m+1,n}u_{m+1,n} \\
&\quad + k^2_{m,n-1}u_{m,n-1} + k^2_{m,n+1}u_{m,n+1}\Big), \\
\mathcal{I}_{h,45^o}\left(k^2u\right) \mid_{x=x_m,y=y_n} &:= \frac{1}{4}\Big(k^2_{m-1,n+1}u_{m-1,n+1} + k^2_{m+1,n-1}u_{m+1,n-1} \\
&\quad + k^2_{m-1,n-1}u_{m-1,n-1} + k^2_{m+1,n+1}u_{m+1,n+1}\Big),
\end{aligned}$$

and approximate $k^2u \mid_{x=x_m,y=y_n}$ by a weighted average:

$$k^2u \mid_{x=x_m,y=y_n} \approx \mathcal{I}_h\left(k^2u\right) \mid_{x=x_m,y=y_n},$$

where

$$\begin{aligned}
\mathcal{I}_h\left(k^2u\right) \mid_{x=x_m,y=y_n} &:= ck^2_{m,n}u_{m,n} + d\mathcal{I}_{h,0^o}\left(k^2u\right) \mid_{x=x_m,y=y_n} \\
&\quad + e\mathcal{I}_{h,45^o}\left(k^2u\right) \mid_{x=x_m,y=y_n},
\end{aligned} \tag{2.3}$$

in which c, d, e are parameters satisfying $c + d + e = 1$.

These yield the rotated 9-point difference approximation for the Helmholtz equation as

$$\Delta_h u \mid_{x=x_m,y=y_n} + \mathcal{I}_h\left(k^2u\right) \mid_{x=x_m,y=y_n} = 0. \tag{2.4}$$

Substituting (2.2) and (2.3) into equation (2.4) and replacing $u_{m+i,n+j}$ with $U_{m+i,n+j}$ $(i, j \in \mathbb{Z}_2 := \{-1, 0, 1\})$ give the rotated 9-point finite difference equation

$$\begin{array}{ccccccc}
 & R_1U_{m-1,n-1} & + & R_2U_{m,n-1} & + & R_3U_{m+1,n-1} \\
+ & R_4U_{m-1,n} & + & R_5U_{m,n} & + & R_6U_{m+1,n} \\
+ & R_7U_{m-1,n+1} & + & R_8U_{m,n+1} & + & R_9U_{m+1,n+1} = 0,
\end{array} \tag{2.5}$$

where the parameters are given by

$$\begin{array}{lll} R_1 := \frac{1-a}{2h^2} + \frac{e}{4}k^2_{m-1,n-1}, & R_2 := \frac{a}{h^2} + \frac{d}{4}k^2_{m,n-1}, & R_3 := \frac{1-a}{2h^2} + \frac{e}{4}k^2_{m+1,n-1}, \\ R_4 := \frac{a}{h^2} + \frac{d}{4}k^2_{m-1,n}, & R_5 := -\frac{2(1+a)}{h^2} + ck^2_{m,n}, & R_6 := \frac{a}{h^2} + \frac{d}{4}k^2_{m+1,n}, \\ R_7 := \frac{1-a}{2h^2} + \frac{e}{4}k^2_{m-1,n+1}, & R_8 := \frac{a}{h^2} + \frac{d}{4}k^2_{m,n+1}, & R_9 := \frac{1-a}{2h^2} + \frac{e}{4}k^2_{m+1,n+1}. \end{array}$$

Note that $U_{m,n}$ is intended to approximate $u_{m,n}$, and the parameters a, c, d, e should be chosen. It is clear that equation (2.5) is a second order difference scheme of the Helmholtz equation (1.1) for arbitrary constants a, c, d and e, if $a \in (0, 1]$ and c, d, e satisfy the condition $c + d + e = 1$. The parameters can be optimized for some purposes. Jo, Shin and Suh [19] provided a group of optimal parameters:

$$a = 0.5461, \quad d = 0.3752, \quad e = -4.0000 \times 10^{-5}. \tag{2.6}$$

The rotated 9-point finite difference equation (2.5) with parameters (2.6) is a good scheme for the Helmholtz equation, its numerical dispersion is very small than that of the conventional 5-point scheme (see, [19]).

To develop the rotated 9-point difference scheme for solving the Helmholtz-PML equation (2.1), we let

$$\begin{aligned} A_{m+\frac{i}{2},n+\frac{j}{2}} &:= A(x_0 + (m - 1 + \tfrac{i}{2})\Delta x, y_0 + (n - 1 + \tfrac{j}{2})\Delta y), \\ B_{m+\frac{i}{2},n+\frac{j}{2}} &:= B(x_0 + (m - 1 + \tfrac{i}{2})\Delta x, y_0 + (n - 1 + \tfrac{j}{2})\Delta y), \\ C_{m,n} &:= C(x_0 + (m - 1)\Delta x, y_0 + (n - 1)\Delta y), \end{aligned}$$

for $i, j \in \mathbb{Z}_3 := \{-2, -1, 0, 1, 2\}$. According to the construction of the rotated 9-point difference method we define

$$\mathcal{L}_h u \mid_{x=x_m,y=y_n} := a\mathcal{L}_{h,0^o} u \mid_{x=x_m,y=y_n} + (1 - a)\mathcal{L}_{h,45^o} u \mid_{x=x_m,y=y_n},$$

where

$$\begin{aligned} &\mathcal{L}_{h,0^o} u \mid_{x=x_m,y=y_n} \\ &:= \frac{1}{h}\Big\{\Big(A_{m+\frac{1}{2},n}\frac{u_{m+1,n} - u_{m,n}}{h} - A_{m-\frac{1}{2},n}\frac{u_{m,n} - u_{m-1,n}}{h}\Big) \\ &\qquad + \Big(B_{m,n+\frac{1}{2}}\frac{u_{m,n+1} - u_{m,n}}{h} - B_{m,n-\frac{1}{2}}\frac{u_{m,n} - u_{m,n-1}}{h}\Big)\Big\}, \end{aligned} \tag{2.7}$$

$$\begin{aligned} &\mathcal{L}_{h,45^o} u \mid_{x=x_m,y=y_n} \\ &:= \frac{1}{\sqrt{2}h}\Big\{\Big(A_{m+\frac{1}{2},n-\frac{1}{2}}\frac{u_{m+1,n-1} - u_{m,n}}{\sqrt{2}h} - A_{m-\frac{1}{2},n+\frac{1}{2}}\frac{u_{m,n} - u_{m-1,n+1}}{\sqrt{2}h}\Big) \\ &\qquad + \Big(B_{m+\frac{1}{2},n+\frac{1}{2}}\frac{u_{m+1,n+1} - u_{m,n}}{\sqrt{2}h} - B_{m-\frac{1}{2},n-\frac{1}{2}}\frac{u_{m,n} - u_{m-1,n-1}}{\sqrt{2}h}\Big)\Big\}, \end{aligned} \tag{2.8}$$

and approximate the first two terms of the left hand side of (2.1) as

$$\Big[\frac{\partial}{\partial x}\Big(A\frac{\partial u}{\partial x}\Big) + \frac{\partial}{\partial y}\Big(B\frac{\partial u}{\partial y}\Big)\Big]_{x=x_m,y=y_n} \approx \mathcal{L}_h u \mid_{x=x_m,y=y_n}.$$

Moreover, $\big(k^2 C u\big) \mid_{x=x_m,y=y_n}$ is approximated by

$$\tilde{\mathcal{I}}_h \big(k^2 u\big) \mid_{x=x_m,y=y_n} := \mathcal{I}_h (k^2 C u) \mid_{x=x_m,y=y_n}. \tag{2.9}$$

These yield the rotated 9-point difference approximation for the Helmholtz-PML equation (2.1) as

$$\mathcal{L}_h u \mid_{x=x_m,y=y_n} + \tilde{\mathcal{I}}_h \big(k^2 u\big) \mid_{x=x_m,y=y_n} = 0. \tag{2.10}$$

To analyze this difference approximation, we introduce the concept of consistency (see, [28]).

Definition 2.1. *Suppose that the partial differential equation under consideration is $\mathcal{L}u = f$ and the corresponding finite difference approximation is $L_{m,n}U_{m,n} = F_{m,n}$ where $F_{m,n}$ denotes whatever approximation which has been made of the source term f. Let $(x_m, y_n) := (x_0 + (m-1)\Delta x, y_0 + (n-1)\Delta y)$. The finite difference scheme $L_{m,n}U_{m,n} = F_{m,n}$ is pointwise consistent with the partial differential equation $\mathcal{L}u = f$ at (x, y) if for any smooth function $\phi = \phi(x, y)$,*

$$(\mathcal{L}\phi - f)\mid_{x=x_m, y=y_n} - [L_{m,n}\phi(x_m, y_n) - F_{m,n}] \to 0 \tag{2.11}$$

as $\Delta x, \Delta y \to 0$ and $(x_m, y_n) \to (x, y)$.

For the rotated 9-point finite difference approximation (2.10) of the Helmholtz-PML equation (2.1), we have the following proposition.

Proposition 2.2. *The rotated 9-point finite difference approximation (2.10) is not pointwise consistent with the Helmholtz-PML equation (2.1).*

Proof. Assume that $x_m \le x < x_{m+1}$ and $y_n \le y < y_{n+1}$. It follows from (2.7), (2.8) and the Taylor theorem that

$$\mathcal{L}_{h,0^\circ}u\mid_{x=x_m, y=y_n} = \frac{\partial}{\partial x}\Big(A\frac{\partial u}{\partial x}\Big) + \frac{\partial}{\partial y}\Big(B\frac{\partial u}{\partial y}\Big) + \mu_1 h^2 + \mathcal{O}(h^3), \tag{2.12}$$

$$\begin{aligned}\mathcal{L}_{h,45^\circ}u\mid_{x=x_m, y=y_n} = {} & \frac{1}{2}\Big\{\Big(\frac{\partial}{\partial x} - \frac{\partial}{\partial y}\Big)\Big(A\Big(\frac{\partial}{\partial x} - \frac{\partial}{\partial y}\Big)u\Big) \\ & + \Big(\frac{\partial}{\partial x} + \frac{\partial}{\partial y}\Big)\Big(B\Big(\frac{\partial}{\partial x} + \frac{\partial}{\partial y}\Big)u\Big)\Big\} + \mu_2 h^2 + \mathcal{O}(h^3),\end{aligned} \tag{2.13}$$

where

$$\begin{aligned}\mu_1 := {} & \frac{1}{24}\Big\{\frac{\partial^3}{\partial x^3}\Big(A\frac{\partial u}{\partial x}\Big) + \frac{\partial}{\partial x}\Big(A\frac{\partial^3 u}{\partial x^3}\Big) + \frac{\partial^3}{\partial y^3}\Big(B\frac{\partial u}{\partial y}\Big) + \frac{\partial}{\partial y}\Big(B\frac{\partial^3 u}{\partial y^3}\Big)\Big\}, \\ \mu_2 := {} & \frac{1}{48}\Big\{\Big(\frac{\partial}{\partial x} - \frac{\partial}{\partial y}\Big)^3\Big(A\Big(\frac{\partial}{\partial x} - \frac{\partial}{\partial y}\Big)u\Big) + \Big(\frac{\partial}{\partial x} - \frac{\partial}{\partial y}\Big)\Big(A\Big(\frac{\partial}{\partial x} - \frac{\partial}{\partial y}\Big)^3 u\Big) \\ & + \Big(\frac{\partial}{\partial x} + \frac{\partial}{\partial y}\Big)^3\Big(B\Big(\frac{\partial}{\partial x} + \frac{\partial}{\partial y}\Big)u\Big) + \Big(\frac{\partial}{\partial x} + \frac{\partial}{\partial y}\Big)\Big(B\Big(\frac{\partial}{\partial x} + \frac{\partial}{\partial y}\Big)^3 u\Big)\Big\}.\end{aligned}$$

Similarly we have

$$\tilde{\mathcal{I}}_h\left(k^2 u\right) = k^2 C u + \mu_3 h^2 + \mathcal{O}(h^4), \tag{2.14}$$

where

$$\mu_3 := \frac{1}{4}(d + 2e)\Big(\frac{\partial^2}{\partial x^2}(k^2 C u) + \frac{\partial^2}{\partial y^2}(k^2 C u)\Big).$$

Combining equations (2.12) − (2.14) yields that the left hand side of the rotated 9-point finite difference approximation (2.10) is equivalent to

$$\begin{aligned}a\Big[\frac{\partial}{\partial x}\Big(A\frac{\partial u}{\partial x}\Big) + \frac{\partial}{\partial y}\Big(B\frac{\partial u}{\partial y}\Big)\Big] + \frac{1-a}{2}\Big[\frac{\partial}{\partial x}\Big((A+B)\frac{\partial u}{\partial x}\Big) + \frac{\partial}{\partial y}\Big((A+B)\frac{\partial u}{\partial y}\Big) \\ + \frac{\partial}{\partial x}\Big((B-A)\frac{\partial u}{\partial y}\Big) + \frac{\partial}{\partial y}\Big((B-A)\frac{\partial u}{\partial x}\Big)\Big] + k^2 C u + \zeta h^2 + \mathcal{O}(h^3),\end{aligned}$$

where $\zeta := a\mu_1 + (1-a)\mu_2 + \mu_3$.

In order to verify this proposition, we need to recall the construction of PML in Section 2. From the PML's formulation, we know that there exists some area satisfying $e_y \equiv 1$ and $e_x \neq 1$. Hence, in such area there hold $A = \frac{1}{e_x}$, $B = e_x$ and

$C = e_x$. Combining the above analysis for the rotated 9-point finite difference approximation (2.10), we have that in this area the left hand side of the approximation (2.10) is equivalent to

$$a\Big[\frac{\partial}{\partial x}\Big(\frac{1}{e_x}\frac{\partial u}{\partial x}\Big)+\frac{\partial}{\partial y}\Big(e_x\frac{\partial u}{\partial y}\Big)\Big]+\frac{1-a}{2}\Big[\frac{\partial}{\partial x}\Big((\frac{1}{e_x}+e_x)\frac{\partial u}{\partial x}\Big)+\frac{\partial}{\partial y}\Big((\frac{1}{e_x}+e_x)\frac{\partial u}{\partial y}\Big)$$
$$+\Big(e_x-\frac{1}{e_x}\Big)\Big(\frac{\partial^2 u}{\partial x\partial y}+\frac{\partial^2 u}{\partial y\partial x}\Big)+\frac{\partial}{\partial x}\Big(e_x-\frac{1}{e_x}\Big)\frac{\partial u}{\partial y}\Big]+k^2e_xu+\zeta h^2+\mathcal{O}(h^3).$$

As there exist the terms $\frac{\partial^2 u}{\partial x\partial y}+\frac{\partial^2 u}{\partial y\partial x}$ and $\frac{\partial u}{\partial y}$, we have the conclusion of this proposition for the area which satisfy both $e_y \equiv 1$ and $e_x \neq 1$. Similar results can be obtained almost everywhere in PML. Therefore, we come to the conclusion of this proposition. □

The above proposition tells us that the rotated 9-point finite difference scheme is not pointwise consistent with the Helmholtz-PML equation. As the convergence of the finite difference scheme requires that the finite difference scheme should be consistent with the Helmholtz-PML equation, the rotated 9-point finite difference approximation to the Helmholtz-PML equation is not good enough.

3. An Optimal 9-point Finite Difference Scheme for the Helmholtz Equation with PML

In this section, we firstly propose a 9-point finite difference scheme which is consistent with the Helmholtz-PML equation. We then analyze the error between the numerical wavenumber and the exact wavenumber, and present global and refined optimization rules for choosing the parameters of the finite difference scheme such that the numerical dispersion is minimized well. Finally we generalize the scheme to the case that different step sizes are used for different variables.

3.1. A Consistent 9-point Difference Scheme. To find a consistent 9-point difference scheme for the Helmholtz equation with PML, we follow the approach of constructing finite difference scheme in [26], which was used for the Helmholtz equation with PML in a semi-infinite two-dimensional strip. Here, we note that, compared with the rotated 9-point finite difference scheme, this method is more easily extended to the case of different step sizes for different variables, and to the case of the Helmholtz-PML equation in three dimension domain.

We let

$$\mathcal{L}_{h,x}u\,|_{(m,n+j)} := \frac{A_{m+\frac{1}{2},n+j}(u_{m+1,n+j}-u_{m,n+j})-A_{m-\frac{1}{2},n+j}(u_{m,n+j}-u_{m-1,n+j})}{h^2}, \tag{3.1}$$

for $j \in \mathbb{Z}_2$, and define

$$\tilde{\mathcal{L}}_{h,x}u\,|_{x=x_m,y=y_n} := b\mathcal{L}_{h,x}u\,|_{(m,n)}+\frac{1-b}{2}\left(\mathcal{L}_{h,x}u\,|_{(m,n-1)}+\mathcal{L}_{h,x}u\,|_{(m,n+1)}\right),$$

where $b \in (0,1]$ is a constant. Then we approximate the first term of the left hand side of (2.1) as

$$\frac{\partial}{\partial x}\Big(A\frac{\partial u}{\partial x}\Big)\,|_{x=x_m,y=y_n} \approx \tilde{\mathcal{L}}_{h,x}u\,|_{x=x_m,y=y_n}.$$

We deal with the approximation of the second term in a similar way, that is,

$$\frac{\partial}{\partial y}\Big(B\frac{\partial u}{\partial y}\Big)\,|_{x=x_m,y=y_n} \approx \tilde{\mathcal{L}}_{h,y}u\,|_{x=x_m,y=y_n}.$$

Let $\tilde{\mathcal{L}}_h := \tilde{\mathcal{L}}_{h,x} + \tilde{\mathcal{L}}_{h,y}$. We obtain the following 9-point finite difference approximation for the Helmholtz-PML equation (2.1)

$$\tilde{\mathcal{L}}_h u \mid_{x=x_m,y=y_n} + \tilde{\mathcal{I}}_h \left(k^2 u\right) \mid_{x=x_m,y=y_n} = 0. \tag{3.2}$$

The next proposition presents the convergence analysis for the 9-point difference scheme (3.2).

Proposition 3.1. *If $b \in (0,1]$ and $c+d+e=1$, then the 9-point finite difference approximation (3.2) is pointwise consistent with the Helmholtz-PML equation (2.1) and is a second order scheme.*

Proof. Assume that $x_m \le x < x_{m+1}$ and $y_n \le y < y_{n+1}$. It follows from the Taylor theorem that

$$\Big[\frac{\partial}{\partial x}\Big(A\frac{\partial u}{\partial x}\Big)\Big] \mid_{x=x_m,y=y_n} = \frac{\partial}{\partial x}\Big(A\frac{\partial u}{\partial x}\Big) + \nu_1 h^2 + \mathcal{O}(h^4), \tag{3.3}$$

and

$$\Big[\frac{\partial}{\partial y}\Big(B\frac{\partial u}{\partial y}\Big)\Big] \mid_{x=x_m,y=y_n} = \frac{\partial}{\partial y}\Big(B\frac{\partial u}{\partial y}\Big) + \nu_2 h^2 + \mathcal{O}(h^4), \tag{3.4}$$

where

$$\nu_1 := \frac{1}{24}\Big[\frac{\partial^3}{\partial x^3}\Big(A\frac{\partial u}{\partial x}\Big) + \frac{\partial}{\partial x}\Big(A\frac{\partial^3 u}{\partial x^3}\Big) + 12(1-b)\frac{\partial^3}{\partial y^2 \partial x}\Big(A\frac{\partial u}{\partial x}\Big)\Big],$$

$$\nu_2 := \frac{1}{24}\Big[\frac{\partial^3}{\partial y^3}\Big(B\frac{\partial u}{\partial y}\Big) + \frac{\partial}{\partial y}\Big(B\frac{\partial^3 u}{\partial y^3}\Big) + 12(1-b)\frac{\partial^3}{\partial x^2 \partial y}\Big(B\frac{\partial u}{\partial y}\Big)\Big].$$

We recall the Taylor expansion of $\tilde{\mathcal{I}}_h\left(k^2 u\right)$, which is given in the equation (2.14), and then revisit the expression of the coefficient μ_3 introduced in the middle of the proof of Proposition 2.2. Therefore, together with equations (3.3) and (3.4), we have that the left hand side of the 9-point finite difference approximation (3.2) is equivalent to

$$\frac{\partial}{\partial x}\Big(A\frac{\partial u}{\partial x}\Big) + \frac{\partial}{\partial y}\Big(B\frac{\partial u}{\partial y}\Big) + k^2 C u + \eta h^2 + \mathcal{O}(h^4), \tag{3.5}$$

where $\eta := \nu_1 + \nu_2 + \mu_3$. From (3.5) and (2.1) we conclude the results of this proposition. □

From the proposition above, we see that the 9-point finite difference scheme (3.2) is a second order scheme for arbitrary constants b, c, d and e, under the conditions $b \in (0,1]$ and $c+d+e=1$. A further observation yields the following proposition.

Proposition 3.2. *In the interior area, the rotated 9-point difference scheme (2.4) and the 9-point difference scheme (3.2) are equivalent if $a = 2b-1$.*

Proof. In the interior area, $A = B = C = 1$, thus the 9-point difference scheme (3.2) becomes

$$\begin{array}{rcccccc} & T_1 U_{m-1,n-1} & + & T_2 U_{m,n-1} & + & T_3 U_{m+1,n-1} \\ + & T_4 U_{m-1,n} & + & T_5 U_{m,n} & + & T_6 U_{m+1,n} \\ + & T_7 U_{m-1,n+1} & + & T_8 U_{m,n+1} & + & T_9 U_{m+1,n+1} = 0, \end{array} \tag{3.6}$$

in which the coefficients are given by

$$\begin{array}{lll} T_1 := \frac{1-b}{h^2} + \frac{e}{4}k^2_{m-1,n-1}, & T_2 := \frac{2b-1}{h^2} + \frac{d}{4}k^2_{m,n-1}, & T_3 := \frac{1-b}{h^2} + \frac{e}{4}k^2_{m+1,n-1}, \\ T_4 := \frac{2b-1}{h^2} + \frac{d}{4}k^2_{m-1,n}, & T_5 := -\frac{4b}{h^2} + (1-d-e)k^2_{m,n}, & T_6 := \frac{2b-1}{h^2} + \frac{d}{4}k^2_{m+1,n}, \\ T_7 := \frac{1-b}{h^2} + \frac{e}{4}k^2_{m-1,n+1}, & T_8 := \frac{2b-1}{h^2} + \frac{d}{4}k^2_{m,n+1}, & T_9 := \frac{1-b}{h^2} + \frac{e}{4}k^2_{m+1,n+1}. \end{array}$$

Comparing the parameters of (2.5) and (3.6) leads to the result of this proposition. □

3.2. Choice Strategies for Optimal Parameters of the Finite Difference Scheme. Since the solution of the Helmholtz equation is oscillating seriously for large wavenumbers, to measure the property of a finite difference scheme, only the convergence order is not enough. In fact, the accuracy of the numerical solution deteriorates with increasing wavenumber k. The phenomenon is the so-called 'pollution effect'. As the result of the 'pollution', the wavenumber of the numerical solution is different from the wavenumber of the exact solution, and this is what is called 'numerical dispersion' (see, [17, 18]). Therefore, to minimize the 'numerical dispersion' is to minimize the error between the numerical wavenumber and the exact wavenumber. If the difference scheme has optimal convergence order, and the parameters are chosen such that the scheme has minimal numerical dispersion in the interior area, then we regard it as an optimal scheme for the Helmholtz-PML equation (see, [24]).

To optimize the 9-point scheme (3.2), we first perform classical dispersion analysis by assuming a plane-wave solution of the form $U(x,y) = e^{-ik(x\cos\theta+y\sin\theta)}$, where θ is the propagation angle from the y-axis. The following analysis is based on the assumption that the wavenumber k is a positive constant. Moreover, let v be the velocity of propagation, λ be the wavelength, and G be the number of gridpoints per wavelength, that is, $G = \frac{\lambda}{h}$. Since $\lambda = \frac{2\pi v}{\omega}$ and $k = \frac{\omega}{v}$, we have $kh = \frac{2\pi}{G}$. Also, denote

$$P := \cos(kh\cos\theta) = \cos\Big(\frac{2\pi}{G}\cos\theta\Big) \quad \text{and} \quad Q := \cos(kh\sin\theta) = \cos\Big(\frac{2\pi}{G}\sin\theta\Big).$$

We firstly presents the relationship between $\big(k^N\big)^2$ and k^2, where k^N represents the numerical wavenumber. Substituting $U_{m,n} := e^{-ik(x_m\cos\theta+y_n\sin\theta)}$ into the equation (3.6), dividing both sides by the factor $e^{-ik(x_m\cos\theta+y_n\sin\theta)}$ and finally applying the Euler formula $e^{ix} = \cos x + i\sin x$ lead to the following equation

$$\begin{aligned} &2T_c\Big(\cos(kh\sin\theta + kh\cos\theta) + \cos(kh\sin\theta - kh\cos\theta)\Big) \\ &+2T_s\Big(\cos(kh\cos\theta) + \cos(kh\sin\theta)\Big) + T_o = 0, \end{aligned} \tag{3.7}$$

where

$$T_c = \frac{1-b}{h^2} + \frac{e}{4}k^2, \quad T_s = \frac{2b-1}{h^2} + \frac{d}{4}k^2, \quad T_o = -\frac{4b}{h^2} + (1-d-e)k^2.$$

By replacing the variable k in the parameters T_o, T_s, T_c with k^N in equation (3.7), we obtain that

$$k^N = \frac{1}{h}\sqrt{\frac{4b + 2(1-2b)(P+Q) + 4(b-1)PQ}{(1-d-e) + \frac{d}{2}(P+Q) + ePQ}}. \tag{3.8}$$

The next proposition presents the error between the numerical wavenumber k^N and the exact wavenumber k for the finite difference scheme (3.2).

Proposition 3.3. *For the 9-point finite difference scheme (3.2), there holds*

$$k^N = k + \left[\frac{d}{8} + \frac{e}{4} - \frac{1}{24} + (\frac{b}{8} - \frac{5}{48})\sin^2(2\theta)\right]k^3h^2 + \mathcal{O}(k^4h^3),\ kh \to 0. \tag{3.9}$$

Proof. Let $\tau := kh$. Therefore, both P and Q in equation (3.8) depend on τ and θ, that is, $P(\tau) = \cos(\tau\cos\theta)$, $Q(\tau) = \cos(\tau\sin\theta)$. In addition, denote

$$\begin{aligned} f_1(\tau) &= 4b + 2(1-2b)\left[P(\tau)+Q(\tau)\right] + 4(b-1)P(\tau)Q(\tau), \\ f_2(\tau) &= (1-d-e) + \frac{d}{2}\left[P(\tau)+Q(\tau)\right] + eP(\tau)Q(\tau). \end{aligned}$$

Applying Taylor expansions for $f_1(\tau)$ and $\frac{1}{f_2(\tau)}$ at the point $\tau = 0$, we have

$$\begin{aligned} f_1(\tau) &= \tau^2 + \frac{1}{12}\Big\{2(b-1) + (1-2b)\left[(\cos\theta)^4 + (\sin\theta)^4\right] \\ &\quad +8(b-1)(\cos\theta\sin\theta)^2\Big\}\tau^4 + \mathcal{O}(\tau^5), \end{aligned} \tag{3.10}$$

$$\frac{1}{f_2(\tau)} = 1 + \left(\frac{d}{4} + \frac{e}{2}\right)\tau^2 + \mathcal{O}(\tau^3). \tag{3.11}$$

In addition, from the equation (3.8), we have

$$\left(k^N h\right)^2 = \frac{f_1(\tau)}{f_2(\tau)}.$$

Together with equations (3.10) and (3.11), we obtain

$$\left(k^N\right)^2 = k^2 + \left[\frac{d}{4} + \frac{e}{2} - \frac{1}{12} + (\frac{b}{4} - \frac{5}{24})\sin^2(2\theta)\right]k^4h^2 + \mathcal{O}(k^5h^3),\ kh \to 0.$$

Based on the above equation, applying the Taylor expansion of the function $\sqrt{1+\tau}$ at the point $\tau = 0$ yields the conclusion of this proposition. □

The above proposition indicates that k^N approximates k in a second order. Moreover, the term associated with k^3h^2 presents the pollution effect, which depends on the wavenumber k, the parameters of the finite difference formula (3.2) and the wave's propagation angle θ from the y-axis.

We next present the relationship of the numerical wavenumber k^N and the exact wavenumber k. Since $h = \frac{2\pi}{Gk}$, we conclude that

$$\frac{k^N}{k} = \frac{G}{2\pi}\sqrt{\frac{4b + 2(1-2b)(P+Q) + 4(b-1)PQ}{(1-d-e) + \frac{d}{2}(P+Q) + ePQ}}. \tag{3.12}$$

Finally, we choose optimal parameters b, d and e by minimizing the numerical dispersion. To do this, we set

$$J(b,d,e;G,\theta) := \frac{G}{2\pi}\sqrt{\frac{4b + 2(1-2b)(P+Q) + 4(b-1)PQ}{(1-d-e) + \frac{d}{2}(P+Q) + ePQ}} - 1 \tag{3.13}$$

for $(b,d,e) \in (0,1] \times \mathbb{R}^2$ and $(G,\theta) \in I_G \times I_\theta$, where I_G and I_θ are two intervals. In general, one can choose $I_\theta := [0, \frac{\pi}{2}]$ and $I_G := [G_{\min}, G_{\max}] = [4, 400]$ (see, [25]). We remark that the interval $\left[0, \frac{\pi}{2}\right]$ can be replaced by $\left[0, \frac{\pi}{4}\right]$ because of the symmetry, and $G_{\min} \geq 2$ based on the Nyquist sampling limit (see, [25]).

It follows from (3.12) that minimizing the error between the numerical wavenumber k^N and the exact wavenumber k is equivalent to minimizing the norm $\|J(b,d,e;\cdot,\cdot)\|_{\infty, I_G \times I_\theta}$, which can be formulated as the following rule for the choice of parameters b, d and e.

Rule 3.4. *(Global choice strategy)*

Given intervals $I_\theta := [0, \frac{\pi}{2}]$ *and* $I_G := [4, 400]$, *choose* $(b, d, e) \in (0, 1] \times \mathbb{R}^2$ *such that*

$$(b, d, e) = \arg\min\{\|J(b, d, e; \cdot, \cdot)\|_{\infty, I_G \times I_\theta} : (b, d, e) \in (0, 1] \times \mathbb{R}^2\}, \tag{3.14}$$

which means (b, d, e) *is a point in* $(0, 1]\times\mathbb{R}^2$ *to minimize the norm* $\|J(b, d, e; \cdot, \cdot)\|_{\infty, I_G \times I_\theta}$.

We next remark on the dispersion equation (3.12) by using the physical meaning of the phase velocity and the group velocity. We consider 1-D scalar wave equation (see, [29])

$$u_{tt} - v^2 u_{xx} = 0,$$

in which v is a positive constant. This equation admits solutions of the form

$$u(x, t) = e^{i(\omega t - kx)}, \tag{3.15}$$

where ω and k satisfy the relation

$$\omega^2 = v^2 k^2, \tag{3.16}$$

which is called the dispersion relation for the differential equation. Now, it is obvious that (3.15) propagates rightward with t at the speed

$$V_{ph} = \frac{\omega}{k}, \tag{3.17}$$

which is called the phase velocity. Energy associated with wavenumber k moves asymptotically at the group velocity (cf. [29])

$$V_{gr} = \frac{\partial \omega}{\partial k}. \tag{3.18}$$

Therefore, in a homogeneous, isotropic continuum, there is no dispersion for the exact solution. Waves travel at the phase velocity $V_{ph} = \frac{\omega}{k} = v$, and energy propagates at the group velocity $V_{gr} = \frac{\partial \omega}{\partial k} = v$. Note that $k = \frac{2\pi}{Gh}$. If we regard the numerical phase velocity and group velocity as $V_{ph}^N := \frac{\omega^N}{k}$ and $V_{gr}^N := \frac{\partial \omega^N}{\partial k}$ respectively, then we have that

$$\frac{V_{ph}^N}{v} = \frac{k^N}{k}, \tag{3.19}$$

and

$$\frac{V_{gr}^N}{v} = \frac{\frac{\partial \omega^N}{\partial k}}{v} = \frac{\frac{\partial (k^N v)}{\partial k}}{v} = \frac{\partial k^N}{\partial k}.$$

They are the so-called normalized numerical phase velocity and group velocity respectively (see, [19, 25]). Moreover, by simple computation,

$$\frac{V_{gr}^N}{v} = \frac{v}{V_{ph}^N} \frac{G}{4\pi} \frac{E}{[(1 - d - e) + \frac{d}{2}(P + Q) + ePQ]^2},$$

where

$$\begin{aligned}
E &:= -[2(1 - 2b)R + 4(b - 1)W]\, L + H\left(\frac{d}{2}R + eW\right), \\
L &:= (1 - d - e) + \frac{d}{2}(P + Q) + ePQ, \\
H &:= 4b + 2(1 - 2b)(P + Q) + 4(b - 1)PQ, \\
R &:= \cos\theta \sin(\frac{2\pi}{G}\cos\theta) + \sin\theta \sin(\frac{2\pi}{G}\sin\theta), \\
W &:= \cos\theta \sin(\frac{2\pi}{G}\cos\theta)\cos(\frac{2\pi}{G}\sin\theta) + \sin\theta\cos(\frac{2\pi}{G}\cos\theta)\sin(\frac{2\pi}{G}\sin\theta).
\end{aligned}$$

According to the above discussion we have the following remark.

Remark 3.5. *If we define the numerical angular frequency and the numerical phase velocity by* $\omega^N := k^N v$ *and* $V_{ph}^N := \frac{\omega^N}{k}$ *respectively, then there holds (3.19), which implies that minimizing the error between the numerical wavenumber* k^N *and the exact wavenumber* k *is equivalent to minimizing the error between normalized numerical phase velocity* $\frac{V_{ph}^N}{v}$ *and one.*

To implement Rule 3.4, we solve (3.14) numerically by using the least-squares method. To do this, we first set $J(b,d,e;G,\theta)=0$, which yields the equation

$$\frac{G^2}{4\pi^2}\frac{4b+2(1-2b)(P+Q)+4(b-1)PQ}{(1-d-e)+\frac{d}{2}(P+Q)+ePQ}=1.$$

Thus, we have that

$$\begin{aligned}&2G^2(1-P-Q+PQ)b+\pi^2(2-P-Q)d+2\pi^2(1-PQ)e\\&=2\pi^2+G^2(2PQ-P-Q).\end{aligned}\tag{3.20}$$

Note that P and Q are functions of G and θ. We choose $\theta=\theta_m=\frac{(m-1)\pi}{4(l-1)}\in I_\theta,\ m=1,2,\ldots,l$, and $\frac{1}{G}=\frac{1}{G_n}=\frac{1}{G_{\max}}+(n-1)\frac{\frac{1}{G_{\min}}-\frac{1}{G_{\max}}}{r-1}\in[\frac{1}{G_{\max}},\frac{1}{G_{\min}}],\ n=1,2,\ldots,r$. Then, equation (3.20) leads to the linear system

$$\begin{bmatrix} S_{1,1}^1 & S_{1,1}^2 & S_{1,1}^3\\ \vdots & \vdots & \vdots\\ S_{1,r}^1 & S_{1,r}^2 & S_{1,r}^3\\ \vdots & \vdots & \vdots\\ S_{m,n}^1 & S_{m,n}^2 & S_{m,n}^3\\ \vdots & \vdots & \vdots\\ S_{l,r}^1 & S_{l,r}^2 & S_{l,r}^3 \end{bmatrix}\begin{bmatrix} b\\ d\\ e\end{bmatrix}=\begin{bmatrix} S_{1,1}^4\\ \vdots\\ S_{1,r}^4\\ \vdots\\ S_{m,n}^4\\ \vdots\\ S_{l,r}^4\end{bmatrix},\tag{3.21}$$

where

$$\begin{aligned}S_{m,n}^1 &:= 2G_n^2\Big[1-\cos\Big(\frac{2\pi}{G_n}\cos\theta_m\Big)-\cos\Big(\frac{2\pi}{G_n}\sin\theta_m\Big)\\&\qquad+\cos\Big(\frac{2\pi}{G_n}\cos\theta_m\Big)\cos\Big(\frac{2\pi}{G_n}\sin\theta_m\Big)\Big],\\ S_{m,n}^2 &:= \pi^2\left[2-\cos\Big(\frac{2\pi}{G_n}\cos\theta_m\Big)-\cos\Big(\frac{2\pi}{G_n}\sin\theta_m\Big)\right],\\ S_{m,n}^3 &:= 2\pi^2\left[1-\cos\Big(\frac{2\pi}{G_n}\cos\theta_m\Big)\cos\Big(\frac{2\pi}{G_n}\sin\theta_m\Big)\right],\\ S_{m,n}^4 &:= 2\pi^2+G_n^2\Big[2\cos\Big(\frac{2\pi}{G_n}\cos\theta_m\Big)\cos\Big(\frac{2\pi}{G_n}\sin\theta_m\Big)\\&\qquad-\cos\Big(\frac{2\pi}{G_n}\cos\theta_m\Big)-\cos\Big(\frac{2\pi}{G_n}\sin\theta_m\Big)\Big].\end{aligned}$$

The coefficient matrix of (3.21) has $l\times r$ rows and 3 columns, thus it is an overdetermined system. Following the paper [25], by choosing $l=10$, $r=100$, and using the least-squares method to solve (3.21), we obtain the optimal parameters for difference scheme (3.2):

$$b=0.7926,\quad d=0.3768,\quad e=-0.0064.\tag{3.22}$$

We call the difference scheme (3.2) with parameters (3.22) as the global optimal 9-point scheme for the Helmholtz-PML equation (or simply the global 9p).

We remark that the above method was used in [25] for choosing optimal parameters of the 25-point finite difference scheme, while the rotated 9-point finite difference scheme proposed in [19] used the L^2-norm of the residual, that is

$$\iint \Big[\frac{V_{ph}^N}{v} - 1\Big]^2 \mathrm{d}G\mathrm{d}\theta.$$

In practical computation, parameters provided in (3.22) seems much better than that obtained by using the L^2-norm, especially for large wavenumbers.

We observe that optimal parameters obtained by Rule 3.4 are roughly chosen. Only one group of parameters is obtained and used to the computation for different frequencies, velocities and step sizes. This may yield much numerical dispersion for large wavenumbers and variable $k(x, y)$ (see examples in Section 4). To reduce the numerical dispersion and improve the accuracy of the difference scheme, we propose the following rule.

Rule 3.6. *(Refined choice strategy)*
Step 1. Estimate the interval $I_G := [G_{\min}, G_{\max}]$.
Step 2. Choose $(b, d, e) \in (0, 1] \times \mathbb{R}^2$ *such that*

$$(b, d, e) = \arg\min\{\|J(b, d, e; \cdot, \cdot)\|_{\infty, I_G \times I_\theta} : (b, d, e) \in (0, 1] \times \mathbb{R}^2\}. \tag{3.23}$$

In general, we can estimate I_G by using *a priori* information before choosing parameters. For example, if the frequency $f \in [f_{\min}, f_{\max}]$ and the velocity $v \in [v_{\min}, v_{\max}]$ then for a given step size h we have $G_{\min} := \frac{v_{\min}}{hf_{\max}}$ and $G_{\max} := \frac{v_{\max}}{hf_{\min}}$. As a result, we shall obtain a group of appropriate parameters for the difference scheme, which is much better than that obtained from the global choice strategy Rule 3.4.

In the following table, we present some groups of refined optimal parameters.

TABLE 1. Refined optimal parameters

I_G	[2.5,3]	[3,4]	[4,5]	[5,6]	[6,8]	[8,10]	[10,400]
b	0.6803	0.7427	0.7840	0.8020	0.8133	0.8219	0.8271
d	0.4444	0.4088	0.3832	0.3712	0.3637	0.3578	0.3540
e	0.0008	-0.0036	-0.0060	-0.0072	-0.0075	-0.0078	-0.0080

Figure 2 shows the normalized phase and group velocity curves for the rotated 9-point difference scheme (2.5) with parameters (2.6) (denoted, in short, by rotated 9p), the 9-point difference scheme (3.2) with global optimal parameters (3.22) (global 9p) and above refined optimal parameters (refined 9p), respectively. In each picture of Figure 2, we plot five curves: one is for $y = 1$, the other four are normalized phase velocity curves or normalized group velocity curves for different propagation angles from the y-axis which include 0^o, 15^o, 30^o and 45^o. We can see that the global 9p has some improvement compared with the rotated 9p, while the refined 9p has much less numerical dispersion than both the rotated 9p and the global 9p. In Figure 2 (b)-(d)-(f), the improvement seems not very clearly, because the optimal parameters are obtained by minimizing the error between the normalized phase velocity and 1, not based on the normalized group velocity (cf. [25]). In addition, as we adopt different optimal parameters for different intervals

I_G, the lines for the refined 9p are not smooth enough (see, Figure 2 (e)-(f)). In the next section, numerical experiments will present to compare the accuracies of these schemes.

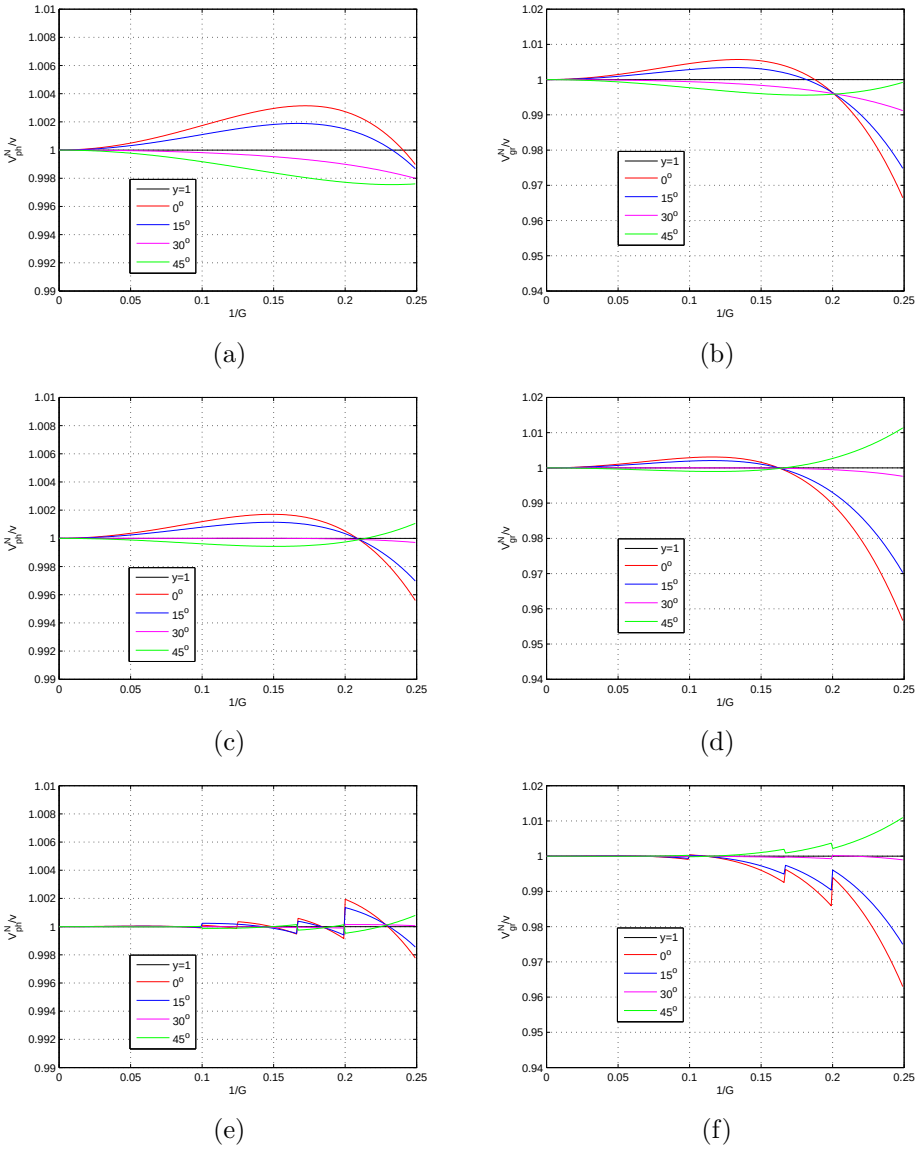

FIGURE 2. (a) Normalized phase velocity curve for the rotated 9p, (b) Normalized group velocity curve for the rotated 9p, (c) Normalized phase velocity curve for the global 9p, (d) Normalized group velocity curve for the global 9p, (e) Normalized phase velocity curve for the refined 9p, (f) Normalized group velocity curve for the refined 9p.

3.3. A Generalization. In practical applications, we usually need to use different step sizes Δx and Δy for variables x and y respectively. In this subsection, we

generalize the 9-point scheme (3.2) to this case and show how to optimize the corresponding parameters.

We denote

$$\begin{aligned}(3.24)\quad &\mathcal{L}_{\Delta x,x}u\mid_{(m,n+j)}\\ &:=\frac{A_{m+\frac{1}{2},n+j}(u_{m+1,n+j}-u_{m,n+j})-A_{m-\frac{1}{2},n+j}(u_{m,n+j}-u_{m-1,n+j})}{(\Delta x)^2},\end{aligned}$$

for $j\in\mathbb{Z}_2$, and define

$$\tilde{\mathcal{L}}_{\Delta x,x}u\mid_{x=x_m,y=y_n}:=b\mathcal{L}_{\Delta x,x}u\mid_{(m,n)}+\frac{1-b}{2}\left(\mathcal{L}_{\Delta x,x}u\mid_{(m,n-1)}+\mathcal{L}_{\Delta x,x}u\mid_{(m,n+1)}\right),$$

where $b\in(0,1]$ is a constant. Then the first term of the left hand side of (2.1) is approximated as

$$\frac{\partial}{\partial x}\Big(A\frac{\partial u}{\partial x}\Big)\mid_{x=x_m,y=y_n}\approx\tilde{\mathcal{L}}_{\Delta x,x}u\mid_{x=x_m,y=y_n}.$$

The approximation of the second term is dealt with in a similar way, that is,

$$\frac{\partial}{\partial y}\Big(B\frac{\partial u}{\partial y}\Big)\mid_{x=x_m,y=y_n}\approx\tilde{\mathcal{L}}_{\Delta y,y}u\mid_{x=x_m,y=y_n}.$$

Let $\tilde{\mathcal{L}}_{\Delta x,\Delta y}:=\tilde{\mathcal{L}}_{\Delta x,x}+\tilde{\mathcal{L}}_{\Delta y,y}$. We obtain the following 9-point finite difference approximation for the Helmholtz-PML equation (2.1)

$$(3.25)\qquad \tilde{\mathcal{L}}_{\Delta x,\Delta y}u\mid_{x=x_m,y=y_n}+\tilde{\mathcal{I}}_h\left(k^2u\right)\mid_{x=x_m,y=y_n}=0.$$

Remark 3.7. *If $c+d+e=1$, then the 9-point finite difference approximation (3.25) is consistent with Helmholtz-PML equation (2.1).*

When $\Delta x=h$, $\Delta y=\gamma h$ (γ is a positive constant), performing classical dispersion analysis to the finite difference method (3.25) yields

$$(3.26)\qquad k^N=\frac{1}{h}\sqrt{\frac{\tilde{W}}{\tilde{L}}},$$

where

$$\begin{aligned}\tilde{W}&:=2b\left(1+\tfrac{1}{\gamma^2}\right)+2\left[1-b\left(1+\tfrac{1}{\gamma^2}\right)\right]\tilde{P}+2\left(\tfrac{1-b}{\gamma^2}-b\right)\tilde{Q}+2(b-1)\left(1+\tfrac{1}{\gamma^2}\right)\tilde{P}\tilde{Q},\\ \tilde{L}&:=(1-d-e)+\tfrac{d}{2}\left(\tilde{P}+\tilde{Q}\right)+e\tilde{P}\tilde{Q},\end{aligned}$$

in which

$$\tilde{P}:=\cos\left(\gamma kh\cos\theta\right)=\cos\left(\gamma\frac{2\pi}{G}\cos\theta\right),\ \tilde{Q}:=\cos\left(kh\sin\theta\right)=\cos\left(\frac{2\pi}{G}\sin\theta\right).$$

As $h=\frac{2\pi}{Gk}$, we conclude that

$$(3.27)\qquad \frac{k^N}{k}=\frac{G}{2\pi}\sqrt{\frac{\tilde{W}}{\tilde{L}}}.$$

Similarly as before, we choose optimal parameters b, d and e by minimizing the numerical dispersion. To do this, we define the functional

$$(3.28)\qquad J_\gamma(b,d,e;G,\theta):=\frac{G}{2\pi}\sqrt{\frac{\tilde{W}}{\tilde{L}}}-1.$$

It follows from (3.27) that minimizing the error between the numerical wavenumber k^N and the exact wavenumber k is equivalent to minimizing the norm $\|J_\gamma(b,d,e;\cdot,\cdot)\|_{\infty,I_G,I_\theta}$.

The corresponding refined choice strategy can be obtained by replacing $\|J(b,d,e;\cdot,\cdot)\|_{\infty,I_G\times I_\theta}$ in Rule 3.6 with $\|J_\gamma(b,d,e;\cdot,\cdot)\|_{\infty,I_G\times I_\theta}$.

Rule 3.8. *(Refined choice strategy II)*
Step 1. Estimate the interval $I_G := [G_{\min}, G_{\max}]$.
Step 2. Choose $(b,d,e) \in (0,1]\times\mathbb{R}^2$ *such that*

$$(b,d,e) = \arg\min\{\|J_\gamma(b,d,e;\cdot,\cdot)\|_{\infty,I_G\times I_\theta} : (b,d,e)\in(0,1]\times\mathbb{R}^2\}. \tag{3.29}$$

To implement Rule 3.8, we set $J_\gamma(b,d,e;G,\theta)=0$ to obtain the equation

$$\begin{aligned} &G^2\left(1+\frac{1}{\gamma^2}\right)\left(1-\tilde{P}-\tilde{Q}+\tilde{P}\tilde{Q}\right)b+\pi^2\left(2-\tilde{P}-\tilde{Q}\right)d+2\pi^2\left(1-\tilde{P}\tilde{Q}\right)e \\ &\quad=2\pi^2+G^2\left[\left(1+\frac{1}{\gamma^2}\right)\tilde{P}\tilde{Q}-\tilde{P}-\frac{1}{\gamma^2}\tilde{Q}\right]. \end{aligned} \tag{3.30}$$

Dealing with the equation (3.30) as we did with the equation (3.20) yields the refined optimal parameters for the finite difference scheme (3.25).

For the convenience of analysis, we also present the normalized numerical phase velocity and group velocity here. The normalized numerical phase velocity is

$$\frac{V_{ph}^N}{v}=\frac{k^N}{k}, \tag{3.31}$$

and the normalized numerical group velocity is

$$\frac{V_{gr}^N}{v}=\frac{v}{V_{ph}^N}\frac{G}{4\pi}\frac{\tilde{K}}{\tilde{L}^2}, \tag{3.32}$$

where

$$\tilde{K}:=\tilde{H}\tilde{L}-\tilde{W}\left[e\left(\tilde{E}\tilde{Q}+\tilde{P}\tilde{F}\right)+\frac{d}{2}\left(\tilde{E}+\tilde{F}\right)\right],$$

in which

$$\begin{aligned} \tilde{H} &:= 2(b-1)\left(1+\tfrac{1}{\gamma^2}\right)\left(\tilde{E}\tilde{Q}+\tilde{P}\tilde{F}\right)+2\left[1-b\left(1+\tfrac{1}{\gamma^2}\right)\right]\tilde{E}+2\left(\tfrac{1-b}{\gamma^2}-b\right)\tilde{F}, \\ \tilde{E} &:= -\gamma\cos\theta\sin\left(\gamma\tfrac{2\pi}{G}\cos\theta\right),\ \tilde{F} := -\sin\theta\sin\left(\tfrac{2\pi}{G}\sin\theta\right). \end{aligned}$$

4. Numerical Experiments

In this section, we present two numerical experiments to illustrate the efficiency of the schemes described in the last section. All the experiments are performed with Matlab 7v on an Intel Xeon (8-core) with 3.33GHz and 96Gb RAM.

4.1. An Numerical Example for the Helmholtz Equation. Consider the Helmholtz equation

$$-\Delta u-k^2u=0,\quad in\ \Omega:=\ (0,1)\times(0,1), \tag{4.1}$$

with boundary conditions

$$iku+\frac{\partial u}{\partial n}=g,\quad on\ \Gamma:=\ \partial\Omega. \tag{4.2}$$

The function g depends on the parameter θ and is given by

$$g(x)=\begin{cases} i(k-k_2)e^{ik_1x_1}, & if\ \ x\in\Gamma_1\ :=\ (0,1)\times(0,0),\\ i(k+k_1)e^{i(k_1+k_2x_2)}, & if\ \ x\in\Gamma_2\ :=\ (1,1)\times(0,1),\\ i(k+k_2)e^{i(k_1x_1+k_2)}, & if\ \ x\in\Gamma_3\ :=\ (1,0)\times(1,1),\\ i(k-k_1)e^{ik_2x_2}, & if\ \ x\in\Gamma_4\ :=\ (0,0)\times(1,0), \end{cases}$$

with $(k_1, k_2) = k(\cos\theta, \sin\theta)$. The exact solution of this problem is

$$u(x) : = e^{i(k_1 x_1 + k_2 x_2)}.$$

This problem was used for measuring the efficiency of numerical methods in [1]. We use it to measure the accuracy for four different schemes, including the conventional 5-point scheme (5p), the rotated 9p, the global 9p and the refined 9p. The error is measured in C-norm, which is defined as: for any complex vector $\mathbf{z} = [z_1, z_2, \ldots, z_M]$,

$$\|\mathbf{z}\|_C := \max_{1 \le j \le M} |z_j|,$$

where $|z_j|$ is the complex modulus of z_j. The parameters in Table 1 are used as refined optimal parameters.

Tables 2, 3 and 4 show the error in the C-norm for different schemes with different gridpoints N per line for the case $\theta = \frac{\pi}{4}$ with $k = 30, 200$ and 500 respectively. From these tables we see that there are significant improvements of the accuracy one by one, and all of the four schemes are second order formulas. Among three 9-point schemes, the refined 9p improves the accuracy most prominently, especially for large wavenumbers. The refined 9p only needs half of the number of gridpoints to obtain the same accuracy of the rotated 9p. Specifically, from Table 3 we see that when $k = 200$, the accuracy of the refined 9p for $N = 129$ is comparable to that of the rotated 9p for $N = 257$, which means that the accuracy of the refined 9p with 4 gridpoints per wavelength is comparable with that of the rotated 9p with 8 gridpoints per wavelength. In addition, from Table 4 we also find that when $k = 500$, the accuracy of the refined 9p with 6 gridpoints per wavelength is comparable with that of the rotated 9p with 13 gridpoints per wavelength.

TABLE 2. The error in the C-norm for $k = 30$

N	33	65	129	257	513
$5p$	0.9743	0.2325	0.0569	0.0142	0.0035
$rotated\ 9p$	0.1537	0.0391	0.0098	0.0025	0.0006
$global\ 9p$	0.1274	0.0330	0.0083	0.0021	0.0005
$refined\ 9p$	0.1186	0.0291	0.0073	0.0018	4.5131e-04

TABLE 3. The error in the C-norm for $k = 200$

N	129	257	513	1025
$5p$	3.7186	2.9475	1.1732	0.2964
$rotated\ 9p$	1.0258	0.4747	0.1298	0.0331
$global\ 9p$	0.5679	0.2154	0.0698	0.0186
$refined\ 9p$	0.4845	0.0861	0.0216	0.0057

Figure 3 gives an intuitive comparison between the rotated 9p, the global 9p and the refined 9p. It is easy to see that for large wavenumber k, the improvement of the refined 9p over other two schemes is very obvious.

Further comparison among the rotated 9p, the global 9p and the refined 9p is given in Figure 4. Figure 4 (a) presents the error in C-norm of three schemes for the case $kh = 1$, and Figure 4 (b) shows the case $kh = 0.5$. The wavenumber k in

TABLE 4. The error in the C-norm for $k = 500$

N	513	601	701	801	901	1025
$5p$	3.0194	3.0026	2.8025	2.7876	2.7878	2.8472
rotated $9p$	1.6202	1.2790	0.9934	0.7810	0.6353	0.4965
global $9p$	0.5798	0.5395	0.4476	0.3767	0.3122	0.2526
$refined$ $9p$	0.1393	0.1554	0.0730	0.0550	0.0429	0.0344

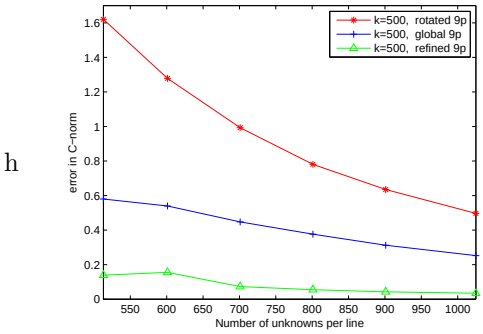

FIGURE 3. Error in C-norm for k=500.

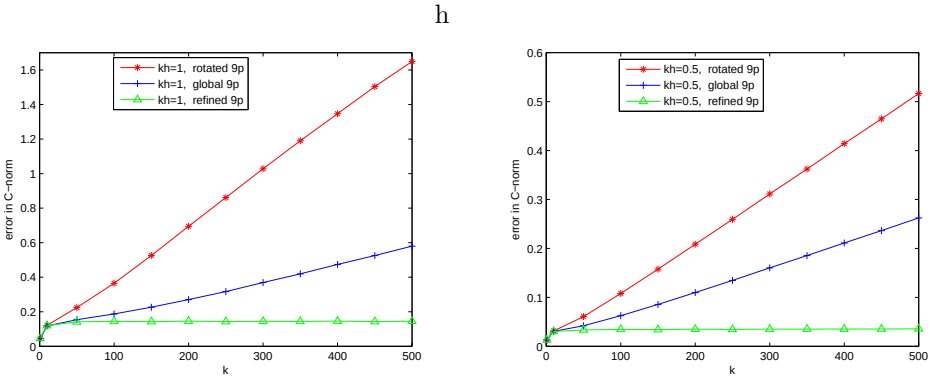

(a) (b)

FIGURE 4. Error in C-norm for $k \in [1, 500]$ and $\theta = \frac{\pi}{4}$: (a) $kh = 1$; (b) $kh = 0.5$.

the two plots varies form 1 to 500, and θ is chosen to be $\frac{\pi}{4}$. Seen from these two pictures, the accuracy of the refined 9p is much higher than that of the global 9p, and it deteriorates much slowly if kh is chosen to be a constant.

All of the experiments above are done with $\theta = \frac{\pi}{4}$. We finally test the dependence on θ of the schemes. Figures 5 (a) and (b) show the corresponding results for $kh = 1$ and $kh = 0.5$ with $k = 500$ respectively, where θ varies among $[0, \pi/2]$. It is clear that, among these three 9-point schemes, the refined 9p's dependence on the wave direction θ is the least and its accuracy is the highest.

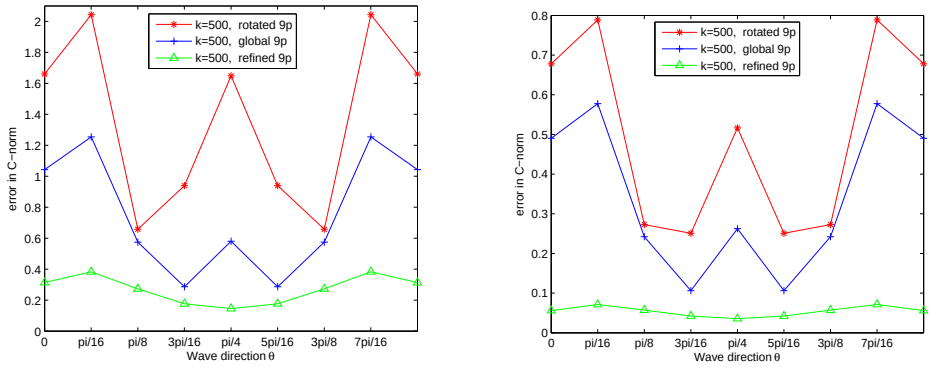

(a) (b)

FIGURE 5. Error in the C-norm for $k = 500$ and $\theta \in [0, \frac{\pi}{2}]$: (a) $kh = 1$; (b) $kh = 0.5$.

Now, we come to our conclusion that the refined 9p is the best scheme, compared to the rotated 9p and the global 9p, and the advantage is more obvious for large wavenumbers.

4.2. Concave Model. To validate the refined optimal 9-point finite difference scheme's availability for the case of variational wavenumbers, which often results from heterogeneous medium, we consider a concave velocity model shown in Figure 6 (a). The domain is $[0m, 2000m] \times [0m, 2000m]$ and there are three velocities: from the top, $v := 1500m/s$, $2000m/s$ and $2500m/s$. A point source $\delta(x - x_s, y - y_s)R(\omega, f_0)$ is located at the point $(x_s, y_s) = (1000m, 800m)$, where $R(\omega, f_0)$ is the Ricker wavelet with

$$R(t, f_0) = (1 - 2\pi^2 f_0^2 t^2) \exp(-\pi^2 f_0^2 t^2),$$

whose dominant frequency is $f_0 = 25Hz$. The grid size is $10m$, the time sampling is $8ms$ and the highest frequency we compute is $60Hz$.

Before computation, we give some remark for the refined optimal parameters. For the concave model, we obtain the refined optimal parameters by two steps. To do computation with the frequency f, we first need to compute $G_{min} = \frac{v_{min}}{fh}$ and $G_{max} = \frac{v_{max}}{fh}$. Then, for the interval $I_G = [G_{min}, G_{max}]$, we obtain the optimal parameters for the interior area with Rule 3.6. For other areas, we just use the same optimal parameters as that of the interior area.

For 201×201 mesh points, we generate snapshots for the wavefield by the rotated 9p and the refined 9p. The monofrequency wavefield (real part) for $f = 25Hz$ obtained by the refined 9p is present in Figure 6 (b). It is easy to see that PML's absorbtion of the outgoing waves is efficient, and almost no boundary reflections exist. Additionally, the upward incident waves, the downward incident waves and transmissive waves are all clear. In the middle velocity layer, the incident waves are interfered with the reflected waves returned from the middle velocity layer's interfaces, and this phenomena obeys Snell's law. In Figure 6 (c), we show snapshot for the time being 400ms generated by the rotated 9p, and Figure 6 (d) shows the corresponding snapshot generated by the refined 9p. Snapshots are given to show the locations of wavefronts at some specific time. The wavefront is the phase

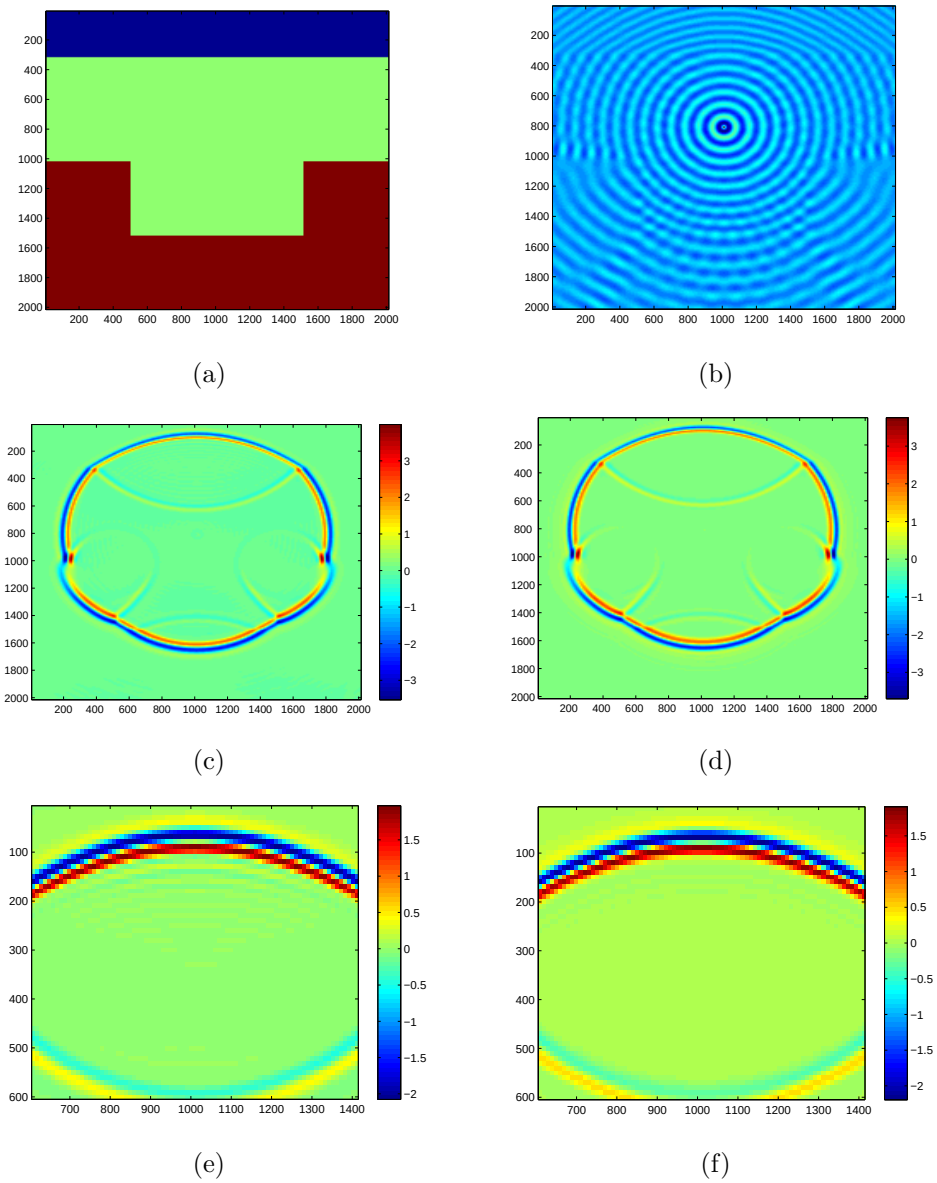

FIGURE 6. (a) Concave model, (b) The real part of the solution for $f = 25Hz$ obtained by the refined 9p, (c) Snapshot generated by the rotated 9p at the time t=400ms, (d) Snapshot generated by the refined 9p at the time t=400ms, (e) Local enlargement for (c), (f) Local enlargement for (d).

velocity surface of wave propagation, and its shape depends on the velocity's distribution. Comparing Figure 6 (c) with Figure 6 (d), we find that they all display the wavefront distortion as the velocity varies, but Figure 6 (d) is much clearer than Figure 6 (c). To see clearly, Figure 6 (e) and Figure 6 (f) present local enlargement for Figure 6 (c) and Figure 6 (d), respectively. From the last two pictures in Figure

6, some unphysical oscillations in the background, such as in depth 200m, can be found in the former, but these do not exist in the latter. Therefore, the efficiency of the refined 9p is confirmed.

5. Conclusions

We summarize and comment on the numerical results. We had proved that the rotated 9-point finite difference scheme is not pointwise consistent with the Helmholtz-PML equation, though it is a popular scheme for the Helmholtz equation. Then, we presented a consistent 9-point difference scheme for the Helmholtz-PML equation. For this method, we gave an error analysis for the numerical wavenumber's approximation of the exact wavenumber, and proposed global and refined choice strategies for choosing optimal parameters based on minimizing the numerical dispersion. Finally, numerical experiments were presented to confirm that the refined 9p is a good choice for the Helmholtz-PML equation, compared with the rotated 9p and the global 9p, as the refined 9p possesses the highest accuracy and the smallest numerical dispersion, especially for large wavenumbers.

Acknowledgments

This research is partially supported by the Natural Science Foundation of China under grants 10771224 and 11071264, the Science and Technology Section of SINOPEC and Guangdong Provincial Government of China through the "Computational Science Innovative Research Team" program.

References

[1] I. Babuška, F. Ihlenburg, E. T. Paik and S. A. Sauter, A genralized finite element method for solving the Helmholtz equation in two dimensions with minimal pollution, *Computer Methods in Applied Mechanics and Engineering,* 128 (1995), 325-359.

[2] I. Babuška and S. A. Sauter, Is the pollution effect of the FEM avoidable for the Helmholtz equation considering high wave numbers? *SIAM Review,* 42 (2000), 451-484.

[3] G. Baruch, G. Fibich, S. Tsynkov and E. Turkel, Fourth order schemes for time-harmonic wave equations with discontinuous coefficients, *Communications in Computational Physics,* 5 (2009), 442-455.

[4] J.-P. Bérenger, A perfectly matched layer for the absorption of electromagnetic waves, *Journal of Computational Physics,* 114 (1994), 185-200.

[5] W. C. Chew, J. M. Jin and E. Michielssen, Complex coordinate stretching as a generalized absorbing boundary condition, *Microwave and Optical Technology Letters,* 15 (1997), 363-369.

[6] R. Clayton and B. Engquist, Absorbing boundary conditions for acoustic and elastic wave equations, *Bulletin of the Seismological Society of American,* 67 (1977), 1529-1540.

[7] R. W. Clayton and B. Engquist, Absorbing boundary conditions for wave-equations migration, *Geophysics,* 45 (1980), 895-904.

[8] A. Deraemaeker, I. Babuška and P. Bouillard, Dispersion and pollution of the FEM sollution for the Helmholtz equation in one, two and three dimensions, *International Journal for Numerical Methods in Engineering,* 46 (1999), 471-499.

[9] P. M. De Zeeuw, Matrix-dependent prolongations and restrictions in a blackbox multigrid solver, *Journal of Computational and Applied Mathematics,* 33 (1990), 1-27.

[10] B. Engquist and A. Majda, Absorbing boundary conditions for the numerical simulation of waves, *Mathematics of Computation,* 31 (1977), 629-651.

[11] Y. A. Erlangga, C. W. Oosterlee and C. Vuik, A novel multigrid based preconditioner for heterogeneous Helmholtz problems, *SIAM Journal on Scientific Computing,* 27 (2006), 1471-1492.

[12] X. Feng and H. Wu, Discontinuous galerkin methods for the Helmholtz equation with large wave number, *SIAM Journal on Numerical Analysis,* 47 (2009), 2872-2896.

[13] Y. Guo and F. Ma, Some domain decomposition methods employing the PML technique for the Helmholtz equation, *Numerical Mathematics A Journal of Chinese Universities,* 31 (2009), 369-384.

[14] I. Harari and E. Turkel, Accurate finite difference methods for time-harmonic wave propagation, *Journal of Computational Physics,* 119 (1995), 252-270.
[15] F. D. Hastings, J. B. Schneider and S.L. Broschat, Application of the perfectly matched layer(PML) absorbing boundary condition to elastic wave propagation, *Journal of Acoustical Society of America,* 100 (1996), 3061-3069.
[16] B. Hustedt, S. Operto and J. Virieux, Mixed-grid and staggered-grid finite-difference methods for frequency-domain acoustic wave modelling, *Geophysical Journal International,* 157 (2004), 1269-1296.
[17] F. Ihlenburg and I. Babuška, Finite element solution of the Helmholtz equation with high wave number, Part I: The h-version of the FEM, *Computers & Mathematics with Applications,* 30 (1995), 9-37.
[18] F. Ihlenburg and I. Babuška, Dispersion analysis and error estimation of galerkin finite element methods for the Helmholtz equation, *International Journal for Numerical Methods in Engineering,* 38 (1995), 3745-3774.
[19] C.-H. Jo, C. Shin and J. H. Suh, An optimal 9-point, finite-difference, frequency-space, 2-D scalar wave extrapolator, *Geophysics,* 61 (1996), 529-537.
[20] J. W. Kang and L. F. Kallivokas, Mixed unsplit-field perfectly matched layers for transient simulations of scalar waves in heterogeneous domains, *Computers & Geosciences,* 14 (2010), 623-648.
[21] J. W. Kang and L. F. Kallivokas, The inverse medium problem in heterogeneous PML-truncated domains using scalar probing waves, *Computer Methods in Applied Mechanics and Engineering,* 200 (2011), 265-283.
[22] R. G. Pratt, C. Shin and G. J. Hicks, Gauss-Newton and full Newton methods in frequency-space seismic waveform inversion, *Geophysical Journal International,* 133 (1998), 341-362.
[23] R. G. Pratt and M. H. Worthington, Inverse theory applied to multi-source cross-hole tompgraphy. Part 1: Acoustic wave-equation method, *Geophysical Prospecting,* 38 (1990), 287-310.
[24] H. Ren, H. Wang and T. Gong, Seismic modeling of scalar seismic wave propagation with finite difference scheme in frequency-space domain, *Geophysical Prospecting for Petroleum,* 48 (2009), 20-27.
[25] C. Shin and H. Sohn, A frequency-space 2-D scalar wave exteapolator using extended 25-point finite-difference operator, *Geophysics,* 63 (1998), 289-296.
[26] I. Singer and E. Turkel, A perfectly matched layer for the Helmholtz equation in a semi-infinite strip, *Journal of Computational Physics,* 201 (2004), 439-465.
[27] I. Singer and E. Turkel, High-order finite difference methods for the Helmholtz equation, *Computer Methods in Applied Mechanics and Engineering,* 163 (1998), 343-358.
[28] J. W. Thomas, *Numerical Partial Differential Equations, Finite Difference Methods*, Springer, New York, 1995.
[29] L. N. Trefethen, Group velocity in finite difference schemes, *SIAM Review,* 24 (1982), 113-136.
[30] S. Tsynkov and E. Turkel, A Cartesian perfectly matched layer for the Helmholtz equation. Absorbing boundaries and layers, domain decomposition methods, *Nova Science Publishers, Huntington, NY,* (2001), 279-309.
[31] E. Turkel and A. Yefet, Absorbing PML boundary layers for wave-like equations, *Applied Numerical Mathematics,* 27 (1998), 533-557.
[32] M. B. Van Gijzen, Y. A. Erlangga and C. Vuik, Spectral analysis of the discrete Helmholtz operator preconditioned with a shifted laplacian, *SIAM Journal on Scientific Computing,* 29(2007), 1942-1958.
[33] Y. Zeng, J. He and Q. Liu, The application of the perfectly matched layer in numerical modeling of wave propagation in poroelastic media, *Geophysics,* 66 (2001), 1258-1266.

† Guangdong Province Key Laboratory of Computational Science, Sun Yat-sen University, Guangzhou 510275, P. R. China.
E-mail: lnsczy@mail.sysu.edu.cn, dongsheng2001@sohu.com, fengw@mail.sysu.edu.cn,

‡ Corresponding author. School of Mathematical Sciences, Shandong Normal University, Jinan 250014, P. R. China.
E-mail: wttxrm@126.com